2002

Mon. Not. R. Astron. Soc. **000**, 2–12 (2002)

Cross-spectral analysis of the X-ray variability of Markarian 421

Y.H. Zhang ⋆
Dipartimento di Scienze, Università dell'Insubria, via Valleggio 11, I-22100 Como, Italy

Accepted . Received ; in original form

ABSTRACT
Using the cross-spectral method, we confirm the existence of the X-ray hard lags discovered with cross-correlation function technique during a large flare of Mrk 421 observed with *Beppo*SAX. For the 0.1–2 versus 2–10 keV light curves, both methods suggest sub-hour hard lags. In the time domain, the degree of hard lag, i.e., the amplitude of the 3.2–10 keV photons lagging the lower energy ones, tends to increase with the decreasing energy. In the Fourier frequency domain, by investigating the cross-spectra of the 0.1–2/2–10 keV and the 2–3.2/3.2–10 keV pairs of light curves, the flare also shows hard lags at the lowest frequencies. However, with the present data, it is impossible to constrain the dependence of the lags on frequencies even though the detailed simulations demonstrate that the hard lags at the lowest frequencies probed by the flare are not an artifact of sparse sampling, Poisson and red noise. As a possible interpretation, the implication of the hard lags is discussed in the context of the interplay between the (diffusive) acceleration and synchrotron cooling of relativistic electrons responsible for the observed X-ray emission. The energy-dependent hard lags are in agreement with the expectation of an energy-dependent acceleration timescale. The inferred magnetic field ($B \sim 0.11$ Gauss) is consistent with the value inferred from the Spectral Energy Distributions of the source. Future investigations with higher quality data that whether or not the time lags are energy-/frequency-dependent will provide a new constraint on the current models of the TeV blazars.

Key words: BL Lacertae objects: general – BL Lacertae objects: individual (Mrk 421) – methods: data analysis – galaxies: active – X-rays: galaxies

1 INTRODUCTION

It has been well established that blazars are extra-galactic sources possessing relativistic jets aligned close to the line of sight, nevertheless, it is still poorly understood how the jets are powered, formed and collimated, and how particles are efficiently accelerated. One of the best observational approaches would be to use temporal and spectral analysis of the emission from the jets. Although blazars are not the unique hosts of jets, being dominated by Doppler effects (causing the observed emission to be enhanced and the timescales shortened), they are the ideal targets for studying jet physics.

The dominant radiation mechanisms in blazars are thought to be synchrotron and inverse Compton by relativistic electrons in a tangled magnetic field, which can reproduce the two peaks of the Spectral Energy Distributions (SEDs) in the $\nu F_\nu - \nu$ diagram: synchrotron radiation is responsible for the low energy peak, while inverse-Compton upscattering by the same population of electrons produces the high energy one (e.g., Urry & Padovani 1995). In such a picture, the blazar family could be unified on the basis of the SEDs whose properties are determined by the bolometric luminosities (Ghisellini et al. 1998).

According to this scenario, the variability of blazars is expected to be energy-dependent, with the highest energy part of each emission component showing the most rapid variations as produced by the highest energy part of the relativistic electron distribution which evolves most rapidly. For high-energy (usually UV/soft X-rays) synchrotron peaked blazars (HBLs), X-rays provide an ideal radiative window for studying the variations because (1) rapid variability indicates that the X-rays arise from the innermost region of the jets, and give direct clues on the central source; (2) synchrotron X-ray emission probes the electrons accelerated to the highest energies, which plausibly have the longest acceleration and the shortest cooling times.

The detected TeV blazars at TeV energies are typical HBLs, including three well-studied classical BL Lac objects, Mrk 421, Mrk 501, and PKS 2155–304. The former two have

⋆ E-mail: youhong.zhang@uninsubria.it

been detected as bright and variable TeV emitters. In particular, Mrk 421 ($z = 0.031$) is the brightest blazar at UV, X-ray and TeV wavelengths. These sources have thus received particular attention as ideal targets for detailed temporal and spectral variability studies in the broadest spectral ranges. Extensive multi-wavelength monitoring campaigns and long looks with various satellites have been conducted.

Intensive monitoring has shown that the synchrotron peak energy up-shifts with flux in these sources (Pian et al. 1998; Fossati et al. 2000b; Tavecchio et al. 2001; Zhang et al. 2002). They have also exhibited quite different variability properties and spectral evolution from flare to flare, indicating that the high energy photons can lead or lag the low energy ones (e.g., Zhang et al. 1999, 2002; Fossati et al. 2000a; Tanihata et al. 2001). The so-called soft lag (lower energy X-ray photons lagging higher energy ones) is consistent with the picture of the energy-dependent cooling time of relativistic electrons—higher energy electrons cool faster. The opposite behavior, i.e., the so-called hard lag (higher energy X-ray photons lagging the lower energy ones) has been found (as not rare) with recent long looks of the three TeV blazars with *Beppo*SAX and ASCA. This "unusual" hard lag has been thought to give direct information on electrons acceleration: it takes longer time for higher energy electrons to accelerate to the radiative energy.

In this paper, through the studies of the time lags in the time and frequency domains, the cross-correlation function (CCF) and the cross-spectral methods are used to re-examine the discovery of the X-ray hard lags during a large flare of Mrk 421 detected by *Beppo*SAX (Fossati et al. 2000a). The latter method was historically used to analyze the X-ray variability of Galactic black hole candidates (GBHCs; e.g., Miyamoto et al. 1988, 1991; Nowak et al. 1999). Recently, Papadakis, Nandra & Kazanas (2001) adopted this technique to study the X-ray variability of a Seyfert galaxy. Since the cross-spectrum can give more information (i.e., the Fourier frequency-dependent time lags) than the CCF can do, it is able to impose stronger constraints on the emission models.

The paper is organized as follows. The light curves of the flare are presented in §2. The characteristic feature of the hard lag is examined by showing the evolutionary behavior of the hardness ratio versus the count rate. In §3 the dependence of hard lags on photon energies is studied with the CCF method incorporating with a model-independent Monte Carlo simulations. We investigate in §4.1 the time lags in Fourier frequency domain using the cross-spectral technique; detailed simulations are performed in §4.2 to investigate the effects of Poisson and red noise, sampling and signal-noise (S/N) ratio of the data sets. In §5.1 we discuss and compare the results derived in time and frequency domains; the physical implications of the results are preliminarily explored in §5.2; we also briefly compare in §5.3 the time lags in different black hole accreting systems. Finally, we present our conclusions in §6.

2 LIGHT CURVES AND HARDNESS RATIOS

*Beppo*SAX (Boella et al. 1997 and references therein) observed Mrk 421 on 21–23 April 1998 as part of a multi-wavelength long monitoring campaign involving *Beppo*SAX, ASCA, RXTE, EUVE, and ground-based TeV observatories (Maraschi et al. 1999; Takahashi et al. 2000). Full details of *Beppo*SAX data reduction have been given in Fossati et al. (2000a). The *Beppo*SAX observations consist of two distinct parts. This work concentrates on the large flare detected on 21 April, of which the light curve are shown in Figure 1a in two energy bands, i.e., 0.1–2 keV (LECS) and 2–10 keV (MECS). For the light curves of the second part of the observation we refer to Fossati et al. (2000a).

Time-resolved spectral analysis for the flare has been performed by Fossati et al. (2000b). One of the interesting results relevant to this work is that the evolution of the flare in the plane of spectral index versus flux follows an anticlockwise loop (see their Figure 5), indicating the presence of an X-ray hard lag. This qualitatively confirmed the discovery of clear hard lag by the CCF techniques (Fossati et al. 2000a).

Time-resolved spectral analysis can be simply performed by considering hardness ratio, which is a simple representation of the two-point spectral index. For this reason, we show in Figure 1b the hardness ratio of 2–10 to 0.1–2 keV versus the 0.1–10 keV count rate, which is binned over the *Beppo*SAX orbital period (~ 5670 s) — the minimum time bin size over which the light curves can be evenly sampled without differentiating exposure efficiency between the LECS and the MECS detectors. It is clear from Figure 1b that the evolution of the flare tracks a well-defined anticlockwise direction, fully consistent with the discovery of the time-resolved spectral analysis.

3 ENERGY-DEPENDENCE OF TIME LAGS

To quantify the hard lags between the low and high energy variations, we calculated the CCF with two techniques suited to unevenly sampled time series: the Discrete Correlation Function (DCF, Edelson & Krolik 1988) and Modified Mean Deviation (MMD, Hufnagel & Bregman 1992), incorporating with a model-independent Monte Carlo simulations taking into account "flux redistribution" (FR) and "random subset selection" (RSS) of the two cross-correlated light curves (Peterson et al. 1998) to statistically determine the significance of any time lags from the cross-correlation peak distribution (CCPD; Maoz & Netzer 1989). Such an procedure suggests that the 3.5–10 keV emission lags the 0.1–1.5 keV one by $2.7^{+1.9}_{-1.2}$ (DCF) and $2.3^{+1.2}_{-0.7}$ (MMD) (68% confidence range with respect to the average of the CCPD; Fossati et al. 2000a).

Here we re-estimate the lag using the *Fisher's z-transformed* DCF (ZDCF; Alexander 1997) method that approximates each DCF point as a normal distribution. We also take into account some more accurate issues: (1) the ZDCF is normalized by the mean and standard deviation of the two cross-correlated light curves using only the data points that actually contribute to the calculation of each lag (White & Peterson 1994), i.e., the so-called "local" CCF (Welsh 1999). With respect to the "standard" CCF that is identically normalized by the mean and standard deviation of the whole time series, the "local" CCF definitely avoids the problem that the DCF amplitudes can be significantly smaller than -1 at some lags, which is commonly seen in the literature (e.g., Tanihata et al. 2001). We also no-

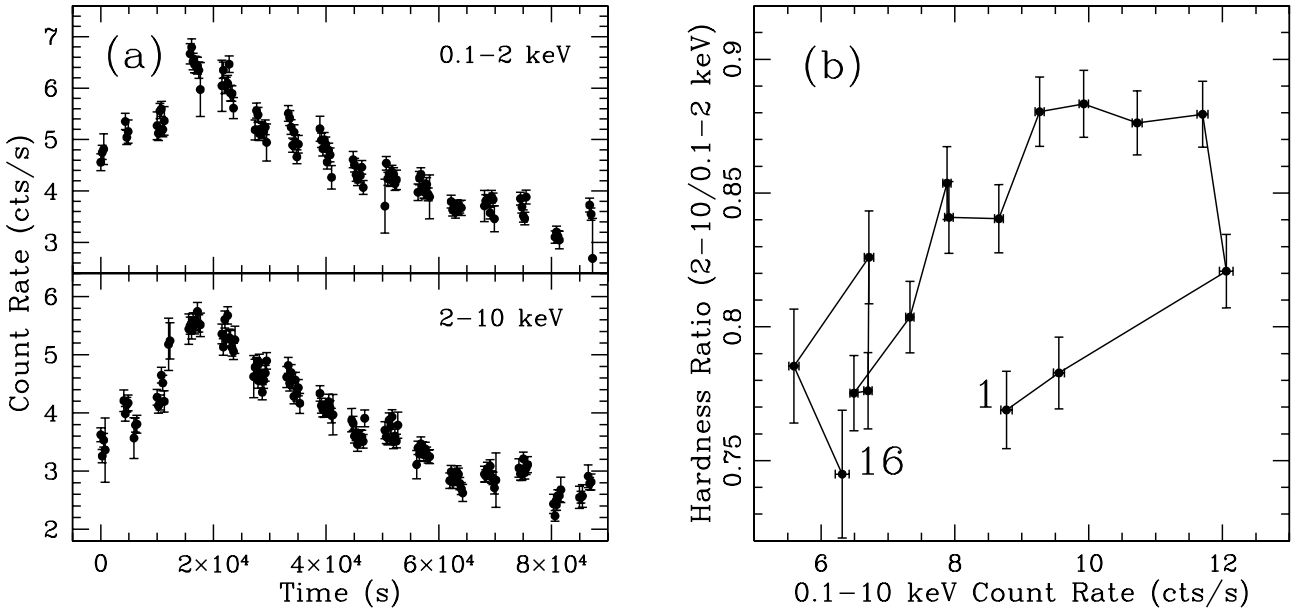

Figure 1. (a) Light curves of the flare of Mrk 421 detected with *Beppo*SAX on 21 April 1998. The data are binned over 256 s. The rising phase of the flare is possibly incomplete. (b) Hardness ratios of the 2–10 keV to the 0.1–2 keV bands as a function of the observed count rates in the 0.1–10 keV band. The data are binned over the *Beppo*SAX orbital period. The first and last point are numbered with the orbital number 1 and 16, respectively, and the evolutionary direction follows the connected line from 1 to 16. An anticlockwise loop can be seen clearly, suggesting that the 2–10 keV emission lags the 0.1–2 keV one.

ticed such problem from the data sets studied here, and from other *Beppo*SAX observations of Mrk 421 and PKS 2155–304, and in particular from an XMM-Newton observation of PKS 2155–304 (Maraschi et al. 2002); (2) the ZDCF is binned by equal points rather than by equal lag step.

The ZDCF of the 0.1–2 versus 2–10 keV bands is shown in Figure 2a. The light curves are binned at 512 s resolution. A positive lag indicates that the higher energy emission lags the lower energy one. One can see that the ZDCF is clearly asymmetric towards the positive lags, while the peak of the ZDCF is near the zero lag. For illustration, we also show in Figure 2a (solid line) the auto-correlation function (ACF) of the 2–10 keV light curve.

It is obvious that there are ambiguities associated with determining such CCF result, in particular for such small time lag. Three techniques to interpret a CCF result exist in the literature: (1) using the time lag corresponding to the actual maximum value ($r_{\rm max}$) of the CCF, $\tau_{\rm peak}$; (2) computing the centroid of the CCF over time lags bracketing $r_{\rm max}$, $\tau_{\rm cent}$; (3) fitting the CCF with a function (e.g., Gaussian) to find the location of the peak, $\tau_{\rm fit}$, which is the technique used in Fossati et al. (2000a). However, $\tau_{\rm peak}$ is not suitable for very small lag compared to the duration of the time series, because it suffers from statistical uncertainties, depends on the binning patterns of both the light curves and the CCF, and does not consider asymmetries of the CCF that is usually seen in AGN variability. Moreover, because of complex CCF shape in this case, $\tau_{\rm fit}$ is not applicable either. We therefore only quote $\tau_{\rm cent}$ throughout the paper.

In Figure 2a, the solid circles indicate all points with r in excess of $0.8r_{\rm max}$, which are used to calculate the centroid of the ZDCF (Peterson et al. 1998). We obtain $\tau_{\rm cent} = 2.87$ ks. We then perform FR/RSS simulations to evaluate its significance. As described in Peterson et al. (1998), a simulation is deemed to have succeeded if $r_{\rm max}$ between the two simulated time series is significant at a level of confidence greater than 95%. For each succeeded trial, $\tau_{\rm cent}$ is recorded. After 2000 runs of successful realizations, we determine the median of $\tau_{\rm cent}$ with 68% confidence range by integrating the CCPD (Figure 2b). The simulations suggest $\tau_{\rm cent} = 2.92^{+2.43}_{-1.50}$ ks.

One obvious issue whether the time lags depend on photon energies can have some important consequences: such energy-dependence may be indeed expected by the energy-dependent acceleration/cooling timescale of relativistic electrons responsible for the observed X-rays. To examine this possibility, we divide the 0.1–10 keV energy range into 5 bands by taking into account each band having similar photon statistics, i.e., 0.1–0.78 keV, 0.78–1.23 keV and 1.23–2 keV (LECS); and 2–3.2 keV, 3.2–10 keV (MECS). Using the FR/RSS simulations, the time lags of the first four lower energy bands are estimated with respect to the 3.2–10 keV energy band. The simulations suggest hard lag for each case. The results are shown in Figure 3 as a function of photon energies. Due to the quality of the data sets used, the errors are quite large, and the possibility of a constant hard lag with no energy-dependence cannot be excluded. Nevertheless, the hard lags appear to be energy-dependent, in the sense that the hard lags of the 3.2–10 keV photons increase with the decreasing energies of the comparison softer photons.

4 FOURIER FREQUENCY-DEPENDENCE OF TIME LAGS

If $X_s(f_i)$ and $X_h(f_i)$ indicate the Fourier transforms of two statistically independent but concurrently measured light curves $x_s(t)$ (soft energy band) and $x_h(t)$ (hard energy band)

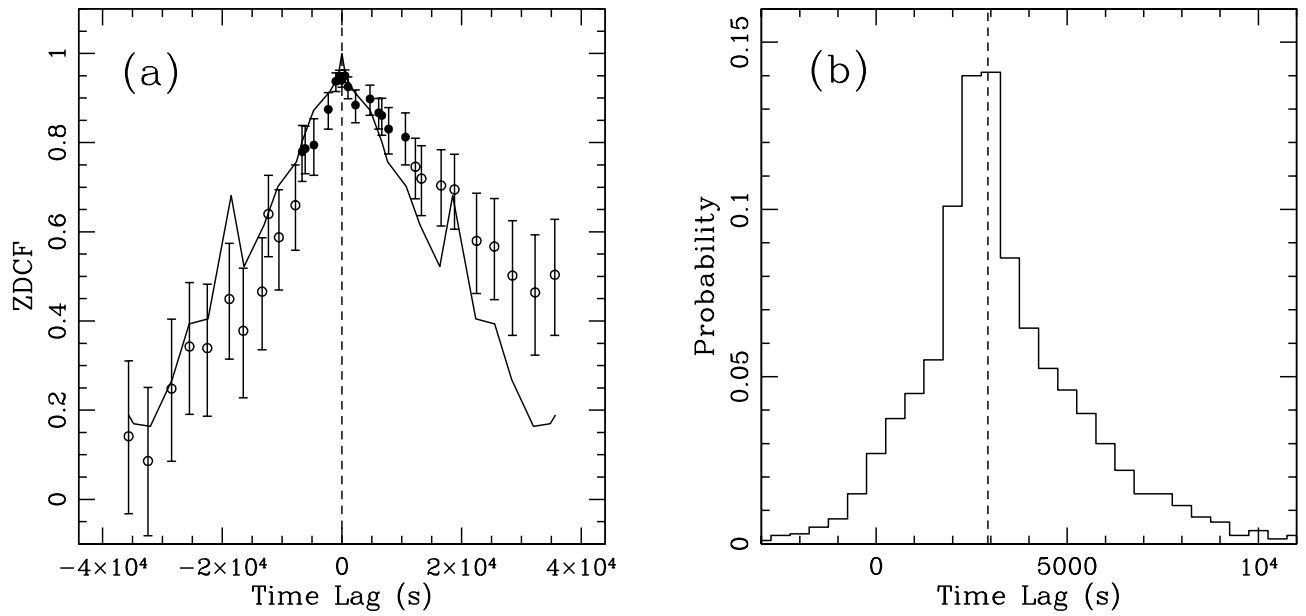

Figure 2. (a) ZDCF (the LECS 0.1–2 keV light curve versus the MECS 2–10 keV one) clearly shows asymmetry towards positive lags while it peaks around zero lag. Such asymmetry is easily visible when one compares the ZDCF with the 2–10 keV ACF (solid line). The solid circles are the ones used to calculate the centroid of the ZDCF, which yield a hard lag of $\tau_{\rm cent} = 2.87$ ks. (b) The corresponding CCPD of (a) built from the FR/RSS simulations, of which the median with 68% confidence level is $\tau_{\rm cent} = 2.92^{+2.43}_{-1.50}$ ks. The vertical dashed line indicates the median of the CCPD.

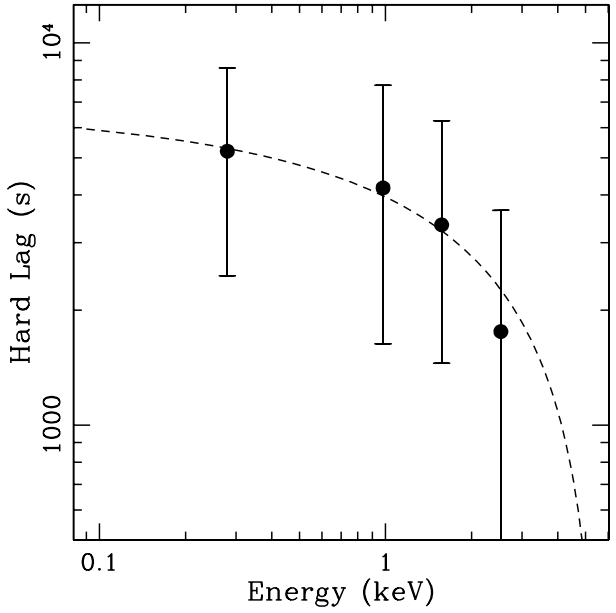

Figure 3. Energy dependence of the hard lag (median of the CCPD) of the 3.2–10 keV photons versus the lower energy ones. The two-sided error bars indicate 68% confidence range with respect to the median of the CCPD. The energies indicate the logarithmically averaged energies of the energy bands by taking into account gradually spectral steepening of the source. The dashed line indicates the best fit with the energy-dependent timescale of a diffusive particle acceleration model (see §5.2 for details).

with N evenly sampled observations ($t = 1\Delta t, 2\Delta t, \ldots, N\Delta t$ with Δt being the bin size of the samples; and $f_i = i/(N\Delta t), i = 1, 2, \ldots, N/2$, is the Fourier frequencies), the cross-spectrum between $x_s(t)$ and $x_h(t)$ is defined as (e.g., Nowak et al. 1999; Papadakis et. al. 2001)

$$I_{s,h}(f_i) = X_s^*(f_i) X_h(f_i)\,, \tag{1}$$

where $X_s^*(f_i)$ is the complex conjugate of $X_s(f_i)$. If $X_h(f_i)$ (or $X_s(f_i)$) is substituted by $X_s(f_i)$ (or $X_h(f_i)$), equation (1) becomes the auto-spectrum, i.e., the spectral power density (PSD) of $x_s(t)$ (or $x_h(t)$). Unlike PSD, the cross-spectrum is a complex function, its argument is defined as the phase spectrum between $x_s(t)$ and $x_h(t)$,

$$\phi_{s,h}(f_i) = \tan^{-1}\left[\frac{{\rm Im}\{I_{s,h}(f_i)\}}{{\rm Re}\{I_{s,h}(f_i)\}}\right]\,, \tag{2}$$

where ${\rm Re}\{I_{s,h}(f_i)\}$ and ${\rm Im}\{I_{s,h}(f_i)\}$ indicate the real and imaginary part of $I_{s,h}(f_i)$, respectively. $\phi_{s,h}(f_i)$ indicates the phase shift, $\phi_s(f_i) - \phi_h(f_i)$, between the fluctuations in $x_s(t)$ and $x_h(t)$ at frequency f_i. The corresponding time shift (lag) is given by

$$\tau_{s,h}(f_i) = \frac{\phi_{s,h}(f_i)}{2\pi f_i}\,, \tag{3}$$

which gives Fourier frequency-dependent time lags, i.e., the lag spectrum, between the variations of the two time series.

4.1 The observed lag spectrum

We extract two pairs of light curves, the 0.1–2 (LECS) versus 2–10 keV (MECS), and the 2–3.2 versus 3.2–10 keV (MECS), respectively. To ensure that the cross-spectrum method is appropriate, evenly sampled data sets are required. We thus use for the analysis two bin sizes correspond-

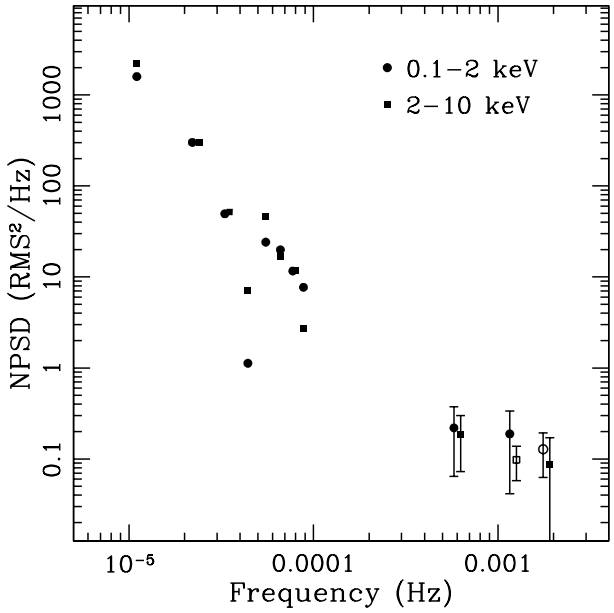

Figure 4. Normalized power spectral density (NPSD) of the 0.1–2 keV and the 2–10 keV light curves. The noise power has been subtracted. The two open symbols indicate negative powers. For clarity, small frequency-offsets have been applied. There are no error estimates for the powers (derived from orbital period-binned light curves) at $f < 10^{-4}$ Hz, while the powers with errors at $f > 10^{-4}$ Hz are derived from the 12 continuous segments of the 256 s binned light curves.

ing to the *Beppo*SAX orbital period and 256 s, respectively. The main goal of such analysis is to examine the results evaluated with the CCF methods (see §3), and to investigate whether or not the source shows frequency-dependent time lags.

There are $N = 16$ points in the orbit-binned light curves. We first estimate individual PSD and cross-spectrum of the two light curves of a pair. The phase spectrum (equation 2) is calculated on the basis of the real and imaginary part of the cross-spectrum, and then the lag spectrum (equation 3). This procedure gives PSDs and lag spectrum of a pair at 8 frequencies in the low frequency range.

For each continuous data segment of the 256 s binned light curves that have no gaps, the PSDs and cross-spectrum of a pair are calculated with the same procedure as above. There are 12 such segments (orbits). We then combine all of them, sort them in order of increasing frequency and group them to 3 (frequency) bins with equal number for both the PSDs and the cross-spectrum. The phase spectrum of the pair are then estimated with the average cross-spectrum. This procedure yields PSDs and lag spectrum of 3 points at high frequency range.

In practice, it is customary to divide the light curves into many segments, compute the PSDs and cross-spectrum for each of them, average PSDs, $\mathrm{Re}\{I_{s,h}(f_i)\}$ and $\mathrm{Im}\{I_{s,h}(f_i)\}$, and/or rebin them by averaging say m consecutive frequency bins to obtain an estimate of the PSDs and phase spectrum with statistical uncertainty. However, our light curves can not match these conditions because of the short duration (i.e., only one single flare was sampled with 16 data points for the orbital period-binned light curve). We believe that this choice is compulsory for the analysis of the TeV sources because the variability properties as discussed in the introduction differ from flare to flare. Accordingly, the statistical uncertainties of the results can not be accounted for by dividing the light curves into segments and rebinning them by averaging consecutive frequency bins. Therefore, at least for the orbital period-binned light curves, the uncertainties on the PSDs and time lags can not be evaluated according to equation [16] of Nowak et al. (1999). It means that there are no error estimates for the results obtained with the orbital period-binned light curves. Even though the results obtained with the 256 s binned light curves have error estimates, low S/N ratio limits the statistical significance.

The resulting PSDs in the 0.1–2 and 2–10 keV energy band are shown in Figure 4 (normalized and noise power subtracted as in Zhang et al. 2002). One can see that the two normalized PSDs (NPSDs) follow power-law shapes with very steep slope, in the sense that the power quickly decreases with increasing frequency, a strong *red noise* feature. There is no clear difference between the two NPSDs.

Due to the limited statistics of the 256 s binned light curves, we only show the observed lag spectrum derived from the orbital period-binned light curves. As commented above, we are discussing here the error-free results. The issues on the errors will be explored with detailed simulations in the next section (§4.2). Figure 5 shows the lag spectrum as a function of Fourier period ($1/f$). A positive value indicates that the component at frequency f in the higher energy band is delayed with respect to the same component in the lower energy band. The 0.1–2/2–10 keV pair (Figure 5a) shows 7 positive (solid circle) and 1 negative (open circle) lags, while the 2–3.2/3.2–10 keV pair (Figure 5b) shows 4 positive and 4 negative values. The dependence of the positive (hard) lags on the periods seems not to be unique: the amplitudes of the lags seem to remain constant or increase with periods. For the four longest periods, all lags are positive with values of $\sim$ 1000–2500 s and $\sim$ 500–1500 s for the 0.1–2/2–10 keV and the 2–3.2/3.2–10 keV pairs, respectively. For the other four periods, the situation is more complicated for both cases. We also mention that the time lags from the 256s-binned pairs are relatively small with either positive or negative signs.

4.2 Simulations

It is obvious that short duration, periodic gaps, sparsely sampling, low S/N ratio and red noise character of the data sets deserve simulations in order to determine the significance and the uncertainties of the error-free results obtained in last section (§4.1).

4.2.1 Poisson noise

We first perform simulations to investigate the effects of Poisson noise (relating to S/N ratio) to the measured lag at each frequency. We use the observed 2–10 keV orbital period-binned light curve as a template. We create a pair of light curves by Gaussian randomly redistributing the fluxes of the light curve using the FR method as adopted in §3 on the basis of the quoted errors on the real light curve. By construction, the pair is identical except for the effects

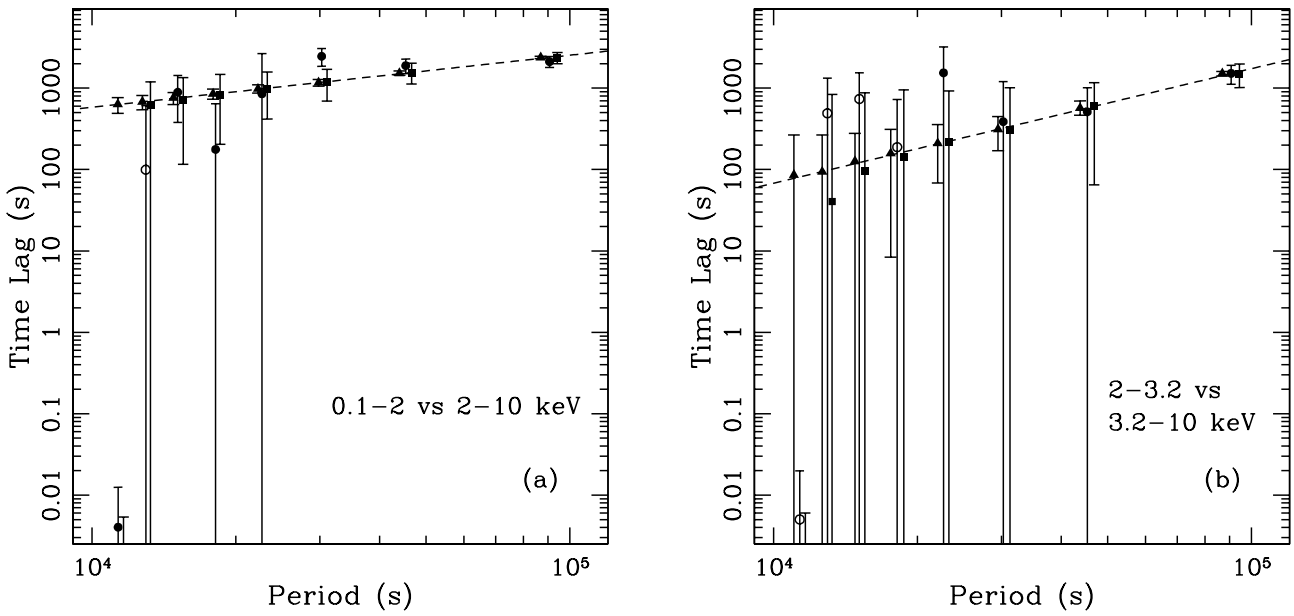

Figure 5. Time lags as a function of Fourier period ($1/f$) derived from the cross-spectrum of (a) 0.1–2 keV versus 2–10 keV; (b) 2–3.2 keV versus 3.2–10 keV. The light curves are 5670 s-binned. The solid (positive) and open (negative) circles are the observed lags of which the errors indicate 68% confidence level due to Poisson noise with respect to the observed lags. The dashed line shows the unweighted best-fit power law model to the observed positive (hard) lags by excluding the negative ones. Moreover, in (a) the point at shortest period is also excluded, and in (b) only the points at the 3 longest periods are used for the fits. The fits do not indicate the accurate phase spectrum of the source, which is only used for the purpose of simulations. Solid squares (5670 s binned light curves) and triangles (256 s binned light curves) are the simulation lags (the medians with 68% confidence levels) by applying the assumed phase spectrum (dashed lines) to the second light curves of the faked pairs (See 4.2.3 for details). For clarity, only 8 points at the longest periods are shown for the case of the 256 s-binned light curves, and period offsets have been applied, and because of very small value the point at the shortest period from 5670 s binned light curves is only seen with part of the upper error bar. The simulations show that densely sampled light curves can well recover the assumed phase spectrum that can be distorted by sparsely sampled light curves.

of Poisson noise, zero lag is expected at each frequency except for a random component contributed by Poisson noise. The pair is analysed with the cross-spectral method in the same way as a real pair, and the lags at each frequency are recorded. After 1000 runs of this process with different sets of random number, the probability distributions (similar to CCPD) are built for the lag at each frequency. Figures 6a,b (solid lines) show such distributions at the two lowest frequencies (i.e., longest periods). As expected, one can see that the lag probability distributions peak at zero. Moreover, the medians of the simulation lags are very close to zero at any frequency, and they are not dominated by positive values as observed in Figure 5a.

As a result, Poisson noise does not result in systematic bias to the observed lags while it introduces an uncertainty. We then investigate how large uncertainty it can introduce. This has been done in the same way as above, but we use light curves at different energy bands rather than those at same energy band. We repeat the above process with the pairs of the orbital period-binned 0.1–2/2–10 keV and 2–3.2/3.2–10 keV light curves, respectively. Figure 6c,d (solid lines) show the probability distributions of the lags at the two lowest frequencies of the 0.1–2/2–10 keV pair, respectively. One can see that the peaks of the lag probability distributions overlaps with the observed ones (vertical dashed lines) while Poisson noise does introduce an uncertainty to the observed lags. Given the sampling pattern (see §4.2.2), the degree of such uncertainty depends on the S/N ratios of the two light curves. After comparing the probability distributions shown with solid lines in Figure 6c,d with those shown with solid lines in Figure 6a,b, we can conclude that the observed lags are not an artifact of Poisson noise. In Figure 5, the error bars on the solid/open circles (i.e., the observed values) show the 68% confidence level of uncertainties introduced by Poisson noise with respect to the observed lags. It can been seen that the relative uncertainty generally increases with decreasing period.

However, it is important to point out, as we will show below, that most of such uncertainties due to Poisson noise as shown above are mainly related to sparsely sampling character of the light curves when one compares the simulation results obtained with faked light curves with different resolutions (given that the light curves have same length and S/N ratio). The probability distributions can be significantly broadened for sparsely sampled light curves, which underestimates the significance of the observed lags.

4.2.2 Red noise

Figure 4 has shown that the source shows strong red noise variations. The unweighted fits with a power-law model to the error-free PSDs suggest a steep slope of about 2.5 for both the 0.1–2 keV and the 2–10 keV PSDs. It is therefore important to investigate the effects of such strong red noise character on the detected lags. To do so, we use randomly generated light curves rather than the observed ones.

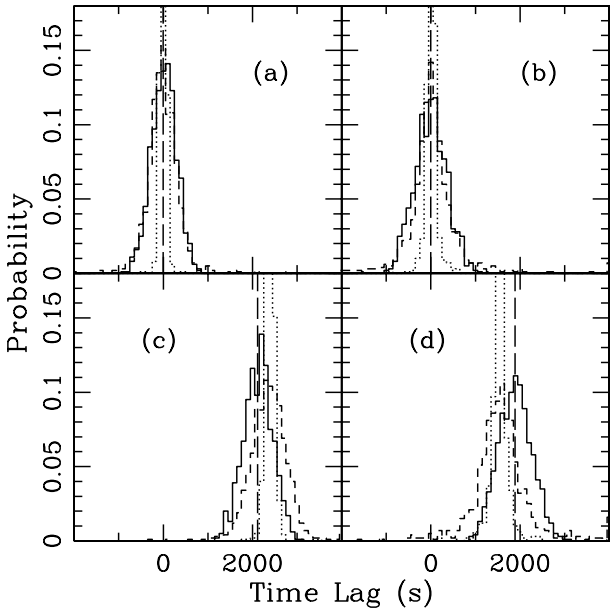

Figure 6. Probability distributions of the simulation lags at the two lowest frequencies (i.e., $f = 1.1 \times 10^{-5}$ Hz (a,c); $f = 2.2 \times 10^{-5}$ Hz (b,d)). (a,b): the solid lines represent the effects of Poisson noise (using the observed 5670 s binned 2–10 keV light curve as a template); the short dashed/dotted lines indicate the effects of red noise (the PSD is assumed to be a power-law model of slope 2.5). The short dashed lines indicate that the faked pairs have the same sampling pattern, mean, variance and Poisson noise as the observed 5670 s binned 0.1–2/2–10 keV pair. The dotted lines are the same as the short dashed ones except for sampling the faked pairs with 354 points of 256 s resolution, and applying the average errors of the observed pair; The vertical long dashed lines indicate zero lags by construction. (c,d): the solid lines are the effects of Poisson noise on the observed 5670 s binned 0.1–2/2–10 keV pair. The vertical long dashed lines indicate the observed lags; the short dashed/dotted lines correspond to those of (a,b), respectively, except for the phase spectrum of the second light curve of the faked pair being delayed on the basis of the best-fit power-law model to the observed 0.1–2/2–10 keV error-free phase spectrum as shown in Figure 5a. The offsets between the peaks of the solid (also the vertical dashed lines) and the short dashed/dotted lines indicate the deviations between the observed and the assumed phase spectrum at the the same frequencies. Note that in all cases the peaks of the short dashed and the dotted lines overlap each other but the latter has been out of the plotting range.

Inverse Fourier transformation from frequency domain to time domain is usually performed to recover the light curves from an assumed PSD model. We use the algorithm of Timmer & König (1995), which randomizes both the amplitude and the phase of the PSD at each Fourier frequency, and is superior to the commonly used "phase only randomisation" approach. Throughout this work, we assume a power-law PSD model with a slope 2.5 appropriate for the source. We consider three cases as follows.

Case 1: with one set of Gaussian distributed random number, we first fake a light curve resembling the sampling pattern of the real orbital period-binned light curves, i.e., the faked light curve has 16 points with 5670 s resolution. We then make this faked light curve become to a pair by scaling it to have the same mean and variance as the real 0.1–2 keV and 2–10 keV light curves, respectively. The two light curves of the faked pair is then Gaussian randomly redistributed using the FR technique on the basis of the quoted errors on the real 0.1–2 keV and 2–10 keV light curves, respectively. The two light curves of the faked pair are therefore identical except for differing mean, variance and Poisson noise, zero lag is then expected at each frequency. The cross-spectral analysis is performed on the faked pair as a real pair, from which the lags are recorded for each frequency. Using different sets of random number, we repeat this process by a number of 1000 to build the probability distributions of simulation lags at each frequency. We show in Figures 6a,b (short dashed lines) such distributions at the two lowest frequencies. One can see that the lag probability distributions due to red noise are similar to those due to Poisson noise only. It means that given the same sampling pattern, the lag uncertainty is mainly associated with Poisson noise rather than red noise. Moreover, same as the effects of Poisson noise, the medians of the simulation lags are likely very close to zero at any frequency, and they are not positive-values dominated as plotted in Figure 5a either. We conclude that the detection of lags from the real pairs of light curves cannot be the result of red noise character of the flare.

Case 2: we repeat the above process with faked light curves having 354 points with 256 s resolution, producing total duration of light curves close to the ones having 16 points with 5670 s resolution. We adopt the same scaling factors as Case 1, and the average Possion noise of the real orbital period-binned 0.1–2 and 2–10 keV light curves, which is similar to those of Case 1, is applied when redistributing the fluxes of the faked light curves, respectively. This set of simulations is used to investigate the effects of different sampling patterns for the deterministic duration of light curves. The results are shown in Figures 6a,b as the dotted lines. One can clearly see that densely sampled light curves yield much narrower lag distributions than the sparely sampled ones do. It means, given the same Poisson noise level, that more sparsely sampled light curves introduce larger uncertainty.

Case 3: Case 2 is repeated with the exact same sets of faked pairs except for doubling the average Poisson noise level. The results show, given sampling pattern and duration, that the larger is Poisson noise level, the larger is the uncertainty.

4.2.3 Phase-shifted red noise

Having established that the observed (phase) lags are not spurious results of Poisson and red noise on the observed data sets, we then investigate what are the "errors" associated with the observed lags. Because the real data sets do not allow us to get proper estimates of the errors directly, we still use faked light curves to investigate how large the errors can be introduced by Poisson and red noise together.

We repeat the three cases in last section (§4.2.2) in the same way, i.e., the same sets of random number, the same scaling factors and Poisson noise levels. The only difference is that one set of random number directly generate a pair of light curves rather than one light curve. For each faked pair, the phase spectrum of the second light curve is delayed with respect to the first one on the basis of the observed

phase spectrum. To do so, an unweighted fit with a power-law model is performed to the observed error-free lag spectrum of the 0.1–2/2–10 keV pair (Figure 5a). The best fit suggests $\tau(t) = 1.60t^{0.64}$ after excluding the negative value and the one at the shortest period, which is shown in Figure 5a (the dashed line). However, we emphasize that such a fit does not really represent the accurate phase spectrum of the flare, it is just used as a reasonable model to investigate the uncertainty and significance of the observed results.

The probability distributions of the simulation lags at the two lowest frequencies are shown in Figures 6c,d, which correspond to those of Figures 6a,b (i.e., the Case 1 and 2 of §4.2.2), respectively. The short dashed and dotted lines show the results derived from the 16 (5670 s resolution) and 354 (256 s resolution) points sampled light curves, respectively. One can see that the assumed lags are easily recovered. The peaks of the lag distributions for the two cases overlap each other while the denser sampled light curves yield narrower distributions. Note that the small offsets between the peaks of the simulation lags (short dashed/dotted lines) and those of the observed ones (solid lines; also see the vertical dashed lines) indicate the deviations of the latter from the best-fit phase spectrum.

In Figure 5a, we show the medians of the simulation lag distributions with 68% confidence level at all the 8 frequencies. The solid squares and triangles represent the results from the case of 16 and 354 points sampled light curves, respectively. For clarity, the results from the 354 points sampled light curves are shown at only the 8 lowest frequencies that correspond to those of the 16 points sampled ones. It can be seen that the simulations of the 16 points sampled light curves recover well the observed lag spectrum at the longest periods. The simulation lags are very similar to the observed ones. Moreover, the dispersions on the simulation values are also similar to those on the observed ones due to Poisson noise only, especially for the two lowest frequencies. This suggests that the uncertainty due to Poisson noise may account for the uncertainty of the observed lags, which resembles the uncertainty on the CCF lags with the FR/RSS simulations. By comparing the simulation results obtained with 16- and 354-points light curves, one can see that sparsely sampled light curves give rise to lag spectrum with much larger uncertainties and distort the true lag in the shortest period.

We repeat the above processes for the observed 2–3.2/3.2–10 keV pair of light curves. We also fit the observed error-free (i.e., unweighted) lag spectrum (Figure 5b) with a power-law model. The fit is performed using only points at the 3 lowest frequencies. The best fit suggests $\tau(t) = 1.62 \times 10^{-4} t^{1.41}$, which is shown in Figure 5b (dashed line). The simulation results are shown in Figures 5b with solid squares and triangles corresponding to the faked light curves having 16 and 354 points, respectively. Similar to the 0.1–2/2–10 keV case, one can clearly see how the sparsely sampled light curves distort the assumed phase spectrum in the sense of both the trends and uncertainties. We conclude that the observed dependence of the lag on frequency has been distorted by the sparsely sampled data sets.

The results corresponding to the Case 3 of §4.2.2 (i.e., using larger Poisson noise level) is that the assumed phase spectra are maintained but with larger dispersions, demonstrating the main effects of low S/N ratios.

As a summary, our simulations show that the observed phase spectra are intrinsic to the source but distorted by the available data quality. The future continuous observations with high resolution and S/N ratio will be able to determine whether or not the time lags in TeV blazars are Fourier frequency-dependent.

5 DISCUSSION

5.1 CCF lag versus phase lag

We reexamined the discovery of hard lags in the X-ray emission during a large flare of Mrk 421 observed with *Beppo*SAX. It was investigated in several ways. The presence of hard lag character is firstly shown with the anticlockwise track in the diagram of hardness ratio versus count rate. We then quantified the hard lags with the CCF method. Finally, we performed an cross-spectral analysis with detailed simulations to evaluate the effects of Poisson and red noise.

The CCF is quite complicated and clearly shows asymmetry and no peak at a lag different from zero. The centroid method suggests that the 2–10 keV emission lags the 0.1–2 keV one by about 3000 s, and the hard lags may be energy-dependent. However, given the data quality in hand and ambiguities in interpreting the complicated shape of the CCF, these results are associated with quite large errors obtained with the FR/RSS simulations. Moreover, the condition that only the CCF points with r in excess of $0.8r_{\max}$ should be used in the determination of $\tau_{\rm cent}$ is just an empirical rule, had one chosen to consider only the few points around the maximum of the CCF (which is close to zero lag) in order to compute $\tau_{\rm cent}$, then the observed "lag" would be close to zero. So, it could be that the "important/real" fact is that the CCF indeed has a maximum at $\sim$ zero lag, and the estimated lag in §3 is just a result of the CCF asymmetry. In other words, the observed asymmetric CCF is difficult to be interpreted since the lag determined from such CCF is not uniquely determined (i.e., it is not easy to understand what exactly this"lag" means). Therefore, in this case the CCF may not address whether there is a "lag" or not, while certainly asymmetric CCF presents significant evidence that the hard photons are delayed with respect to the soft ones.

One possibility that may produce the complicated CCF shape is that the peak of the CCF is possibly dominated by the fastest variations while the asymmetry may be caused by the relative delays of the variations on the longer timescales (e.g., Papadakis et al. 2001). This fact implies that the variations of different periods in various energy bands may not be delayed by the same amount. This further implies that the CCF may always not be the applicable method to correctly address such a situation. The observed CCF lag in such a situation may be difficult to understand/interpret, but could be still important. As an alternative technique to examines the time lag, only the cross-spectral technique may actually reveal the "real" situation. However, the periodic gaps prevent us from performing a full Fourier transformation. The orbital period-binned data sets (only 16 points) therefore yield the observed lag spectra with rather large uncertainties, and the dependence of the lags on frequency is not yet clear. Nevertheless, the detection of statistically significant hard lags between the light curves at the lowest frequen-

cies, which cannot be the result of red noise or Poisson noise effects, assures that the character of hard lag is not problematic. The detailed simulations show that the future higher quality data with higher resolution and S/N ratio, which can be available with Chandra and XMM-Newton, will be able to construct reliable frequency-dependent time lags.

By taking into account the points raised above for the CCF, a direct comparison between the lags obtained with the two different methods is not applicable in this case. Had the CCF and phase lags been uniquely defined, the former should be the average of the latter over the probed frequency range. However, whether two light curves with frequency-dependent time lags will also show a CCF with a "fixed lag" is not clear yet, in fact it is not clear what this "CCF lag" really means. The CCF may have a "fixed" lag if the lag spectrum were frequency-independent, i.e., $\tau(f) = \tau_{\rm CCF} =$ constant. The cross-spectral method may therefore be really superior to the commonly used CCF methods when one investigates time lags.

5.2 Implications of the hard lag

Intensive long looks of the three TeV blazars with *Beppo*SAX and ASCA have revealed that the inter-band X-ray time lags differ significantly from flare to flare. Both soft and hard lags were found, and show dependence on photon energies. Such complex changes of the time lags in these sources have been ascribed to relative changes of acceleration and synchrotron cooling timescales, $t_{\rm acc}$ and $t_{\rm cool}$, of relativistic electrons (e.g., Kirk, Rieger & Mastichiadis 1998). $t_{\rm acc}$ and $t_{\rm cool}$ is electron (in turn photon) energy-dependent: it is such dependence that might produce the complexities of the observed energy-dependent time lags. It is possible that relativistic electrons are accelerated at shock fronts taking place in jets. The widely discussed diffusive shock acceleration in particular (e.g., Drury 1983; Blandford & Eichler 1987) could be the mechanism responsible for electron acceleration during the flare of Mrk 421 studied in this work. In such hypothesis, $t_{\rm acc}$ and $t_{\rm cool}$ in the observer's frame are expressed as (Zhang et al. 2002)

$$t_{\rm acc}(E) = 9.65\times10^{-2}(1+z)^{3/2}\xi B^{-3/2}\delta^{-3/2}E^{1/2} \quad {\rm s}\,, \qquad (4)$$

$$t_{\rm cool}(E) = 3.04\times10^{3}(1+z)^{1/2}B^{-3/2}\delta^{-1/2}E^{-1/2} \quad {\rm s}\,, \qquad (5)$$

where E is the observed photon energy in unit of keV, B and δ are the magnetic field and the Doppler factor of the emitting region, respectively. ξ is the acceleration parameter indicating the acceleration rate of electrons. One can see that both $t_{\rm acc}$ and $t_{\rm cool}$ depend on photon energies but in the *opposite* sense, i.e., the lower energy photons correspond to electrons with shorter acceleration but longer cooling timescales than the higher energy photons do. If the acceleration is instantaneous, (i.e., $t_{\rm acc} \ll t_{\rm cool}$, which corresponds to the case of instantaneous injection of electrons), cooling dominates the variability and the soft lag is expected as

$$\tau_{\rm soft}(E) = t_{\rm cool}(E) - t_{\rm cool}(E_0) \qquad (6)$$

If instead the acceleration is slower and comparable with cooling (i.e., $t_{\rm acc} \sim t_{\rm cool}$), it takes longer time for higher energy electrons to accelerate to the radiative energy, acceleration dominates the system and the hard lag is expected as

$$\tau_{\rm hard}(E) = t_{\rm acc}(E_0) - t_{\rm acc}(E) \qquad (7)$$

where E_0 is the referenced energy at which the lag is measured, and $E < E_0$. One can see that the observed inter-band hard (soft) lag is defined as the difference of $t_{\rm acc}$ ($t_{\rm cool}$) at different energies, from which the physical parameters of the emitting region can be constrained (see Zhang et al. 2002 for details).

Moreover, it is interesting to note that $t_{\rm acc}$ and $t_{\rm cool}$ have the same dependence on B, the ratio of $t_{\rm acc}$ to $t_{\rm cool}$ is thus independent of B. We then have

$$\begin{aligned} t_{\rm acc}(E)/t_{\rm cool}(E) &= 3.17\times10^{-5}(1+z)\xi\delta^{-1}E \\ &= 0.32\times(1+z)\xi_5\delta_1^{-1}E\,, \end{aligned} \qquad (8)$$

where ξ_5 and δ_1 are in unit of 10^5 and 10, respectively. One can see that whether a flare shows soft or hard lags at the considered energy depends on the (energy-dependent) ratio of $t_{\rm acc}/t_{\rm cool}$ (see also Zhang et al. 2002 for an extensive discussion). If one knows $t_{\rm acc}/t_{\rm cool}$ at particular energies (e.g., the maximum synchrotron emitting energy, $E_{\rm max}$, where $t_{\rm acc}/t_{\rm cool} \sim 1$; or the energy where the soft lag changes to the hard lag along the studied energy band), equations (6)–(8) can uniquely determine the main parameters of the emitting region, i.e., B, δ and ξ.

It is worth noting that the effects related to particle acceleration (i.e., the hard lag from point view of observation) are observable only if the system is observed at energies close to $E_{\rm max}$ where $t_{\rm acc} \sim t_{\rm cool}$ (Kirk et al. 1998), indicating a relatively low acceleration rate. It can been seen from Equation (8) that ξ is the key parameter to modulate the variability pattern of a flare since δ is thought to be always the order of $\sim$ 10–25. The value of ξ is poorly known, but changes of ξ provide clues on changes of the shock parameters. Because of the independence of $t_{\rm acc}/t_{\rm cool}$ on B, by assuming $E_{\rm max}$ (i.e., the maximum electron energy, $\gamma_{\rm max}$ which can be accelerated by considering the balance between acceleration and cooling), ξ can be constrained without knowing B (for δ in a small range). On the basis of the commonly assumed parameters ($\gamma_{\rm max} \sim 10^5$, $B \sim 0.1$ Gauss, and $\delta \sim 10$) of the emitting region to account for the SEDs of the Tev blazars (e.g, Kirk et al. 1998; Tavecchio et al. 1998; Fossati et al. 2000b; Kino et al. 2002), the characteristic maximum synchrotron energy as seen in the observer's frame, $E_{\rm max} = 3.7\times10^6\delta B\gamma_{\rm max}^2$ Hz, emitted by the electrons with $\gamma_{\rm max}$, is at the order of a few keV. We then reasonably assume $E_{\rm max} \sim 10$ keV for the flare discussed here. Using Equation (8) and assuming that $\delta \sim 10$ and $t_{\rm acc} = t_{\rm cool}$ at $E_{\rm max} = 10$ keV, ξ is estimated to be $\sim 3.06\times10^4$. Moreover, if the energy-dependent hard lags shown in Figure 3 can be interpreted by $t_{\rm acc}(E)$, we can fit it using Equation (7). The best fit is shown in Figure 3 as the dashed line. It can be seen that $t_{\rm acc}(E)$ fits reasonably well the observed energy-dependent hard lags, supporting the assumption that the flare is dominated by $t_{\rm acc}$. The best fit gives $B\delta\xi^{-2/3} = 1.08\times10^{-3}$ Gauss. If the above values of δ and ξ were assumed, we then have $B \sim 0.11$ Gauss, which is self-consistent with the value used in simulating this flare by Fossati et al. (2000b) and the usual range of B obtained

by fitting the SEDs, i.e., $\sim$ 0.1–0.3 Gauss for the three TeV sources (e.g., Ghisellini, Celotti & Costamante 2002)

With the parameters inferred above, in the observer's frame, $t_{\rm acc}$ and $t_{\rm cool}$ is $\sim 8.46\times10^3$ s at 10 keV; while $t_{\rm acc}$ is $\sim 2.68\times10^3$ s, $t_{\rm cool}\sim 2.68\times10^4$ s, and then $t_{\rm acc}\sim 0.1t_{\rm cool}$ at 1 keV. One can see from Figure 1a that the flare shows quasi-symmetric profile of the rise and decay timescale of $\sim 5\times10^4$ s, which may indicates the light-crossing time ($t_{\rm cross}\sim R/(\delta c)$) across the emitting region. It is then obvious that both $t_{\rm acc}$ and $t_{\rm cool}$ are smaller than $t_{\rm cross}$ in the high energy band, while $t_{\rm cool}$ becomes comparable to $t_{\rm cross}$ in the soft band. Accordingly, the observed emission should be a superposition from different parts of the emitting region with the electron distribution at different stages of evolution. Then the time profile of each variation is not directly observable, but more visible soft lags in the case of $t_{\rm acc}\ll t_{\rm cool}$ are obtained by taking into account the light-crossing time effects (Chiaberge & Ghisellini 1999). By analogy, the light-crossing time effect introduces observable hard lag in the case of $t_{\rm acc}\sim t_{\rm cool}$.

5.3 Comparison with other black hole accreting systems

The X-ray hard lag observed in Mrk 421 is phenomenally similar to those observed in the X-ray variability of GBHCs and Seyfert galaxies. The CCFs of GBHCs (e.g., see Maccarone, Coppi, & Poutanen 2000 for Cyg X–1; Smith & Liang 1999 for GX 339–4) and Seyfert galaxies (e.g., see Lee et al. 2000 for MCG–6-30-15; Papadakis & Lawrence 1995 for NGC 4051; Nandra & Papadakis 2001 for NGC 7469) also clearly show asymmetries towards hard lags. As discussed in §5.1, this suggests that in these sources the relationships between the variations in different energy bands are not simply a "fixed" lag either. This has led to the fact that recent lag determinations in GBHCs have concentrated in Fourier frequency domain. A number of investigations have shown that in GBHCs the dependence of hard lag on frequency can approximate as $\tau(f)\propto 1/f$ with a break at the lowest frequency range (e.g., see Nowak et al. 1999 for Cyg X–1) while such dependence is generally far more complicated. The hard lags in GBHCs also depend photon energies (Miyamoto et al. 1998). In comparison, the Seyfert galaxy NGC 7469 also approximately exhibit $\tau(f)\propto 1/f$ relation (Papadakis et al. 2001). Although Mrk 421 (§4) does not show reliable Fourier frequency-dependent hard lags (possibly due to the data quality), it is still worth mentioning the evidence of similar dependence. Further investigations of such dependence are therefore essential to blazars, and to AGNs in general.

However, the mechanisms producing the X-ray emission and hard lag are rather different. In Mrk 421, synchrotron radiation of nonthermal relativistic electrons is responsible for the observed X-rays, and higher energy photons lag lower energy ones because electrons responsible for higher energy emission need longer time to be accelerated to the observed window. In contrast, in GBHCs and Seyfert galaxies, the production of the X-ray emission is thought to be due to thermal Comptonization of soft photons by hot, thermal electrons, and the hard lag originates either from seed soft photons (because higher energy photons have to undergo more scatterings in the Comptonizing plasma before escape; e.g., Kazanas, Hua & Titarchuk 1997; Hua, Kazanas & Titarchuk 1997) or from the hot Comptonizing cloud itself (because of the changes of the energy dissipation rate; e.g., Poutanen & Fabian 1999).

The frequency-dependence of hard lags has been demonstrated to be a powerful tool in constraining variety of specific models responsible for the the X-ray emission and the associated variability in GBHCs and Seyfert galaxies (Papadakis et al. 2001; See also Poutanen 2001 for a review). However, our interpretation for the hard lag in Mrk 421 and the associated parameter estimates of the emitting region (§5.2) based only on the results from the CCF lags. Since the present work demonstrates that the lag between the variations at different energy bands may be more complicated than the existence of a fixed "lag", more sophisticated models, which will address the presence of frequency-dependent time lags, are needed in order to describe the variability pattern of the source at different energy bands. Moreover, the issue that whether the soft lags in TeV blazars show frequency-dependence is also crucial and worthing investigations. The current blazar models have not yet taken into account the issue of the frequency-dependence of time lags. Therefore, Fourier frequency-dependence of either soft or hard lag, if exist and confirmed, will certainly present a new constraint on the blazar models, specifically, on the TeV blazar models, i.e., the formation and structure of the shocks, particle acceleration and cooling in blazar jets.

6 CONCLUSIONS

X-ray observations have been a powerful diagnostic for the physical processes taking place in the vicinity of the central engines of blazars. *Beppo*SAX observed a well-defined flare of Mrk 421 on 21 April 1998, from which an X-ray hard lag was discovered in a blazar. We investigated with different methods the hard lag character of the flare, and discussed the relevant physical implications.

We examined the conditions that may produce the hard lag variability pattern. For the first time, the energy-dependent acceleration time is assumed to be account for the energy-dependent hard lags. $\xi\sim 3.06\times10^4$ is suggested if the maximum characteristic energy of synchrotron emission were $\sim$ 10 keV, where $t_{\rm acc}\sim t_{\rm cool}$. By fitting the energy-dependent hard lags using the energy-dependent acceleration timescale of relativistic electrons, we found $B\sim 0.11$ Gauss, which is self-consistent with the values inferred from the SEDs. We then deduced that the hard lags are caused by $t_{\rm acc}\sim t_{\rm cool}$, and $t_{\rm acc}$ is energy-dependent.

Finally, we emphasize that our interpretation is based on the simplest scenario. We consider only $t_{\rm acc}$ and $t_{\rm cool}$ without any other complexities involved, in particular the simplified interpretation did not take into account the Fourier frequency-dependence of hard lags (if observably confirmed). However, to understand the relationship between electron acceleration/cooling and time variability, such a study should be qualitatively meaningful, but more accurate analysis needs detailed numerical simulations involving energy-dependent electron acceleration timescale and information of the frequency-dependence of time lags. More importantly, even though there is no doubt about the

sign of hard lag, the results presented in this work are still suggestive, and need further confirmation with higher quality data. Further investigations that whether or not the time lags are energy- and Fourier frequency-dependent will put important implications for the blazar models.

Acknowledgments

The author would like to thank Annalisa Celotti and Aldo Treves for carefully reading the manuscript and stimulating comments. The anonymous referee is thanked for constructive comments which led to significantly improve the depth and presentation of this work. This research has made use of the standard online archive provided by the *Beppo*SAX Science Data Center (SDC). Italian MUIR is acknowledged for financial support.

REFERENCES

Alexander T., 1997, in Astronomical Time Series, eds. D. Maoz, A. Sternberg and E.M. Leibowitz (Dordrecht:Kluwer), p.163
Blandford R., Eichler D., 1987, Phys. Rep., 154, 1
Boella G., et al., 1997, A&AS, 122, 299
Chiaberge M., Ghisellini G., 1999, MNRAS, 306, 551
Drury L.O'C., 1983, Rep. Prog. Phys., 46, 973
Edelson R. A., Krolik J. H., 1988, ApJ, 333, 646
Fossati G. et al., 2000a, ApJ, 541, 153
Fossati G. et al., 2000b, ApJ, 541, 166
Ghisellini G., Celotti A., Fossati G., Maraschi L., Comastri A., 1998, MNRAS, 301, 451
Ghisellini G., Celotti A., Costamante L., 2002, A&A, 386, 833
Hua X.M., Kazanas D., Titarchuk L., 1997, ApJ, 482, L57
Hufnagel B. R., Bregman J. N., 1992, ApJ, 386, 473
Kazanas D., Hua X.M., Titarchuk L, 1997, ApJ, 480, 735
Kino M., Takahara F., Kusunose M. 2002, ApJ, 564, 97
Kirk J., Rieger F., Mastichiadis A., 1998, A&A, 333, 452
Lee J.C., Fabian A.C., Reynolds C.S., Brandt W.N., Iwasawa, K., MNRAS, 318, 857
Maccarone T.J., Coppi P.S., Poutanen J., 2000, ApJ, L107
Maoz D., Netzer H., 1989, MNRAS, 236, 21
Maraschi L. et al., 1999, ApJ, 526, L81
Maraschi L. et al., 2002, in New visions of the X-ray Universe in the XMM-Newton and Chandra Era, ed. F. Jansen, in press (astro-ph/0202418)
Miyamoto S., Kitamoto S., Mitsuda K., Dotani T., 1988, Nat, 336, 450
Miyamoto S., Kimura K., Kitamoto S., 1991, ApJ, 383, 784
Nandra K., Papadakis I.E., 2001, ApJ, 554, 710
Nowak M.A., Vaughan B.A., Wilms J., Dove J.B., Begelman M.C., 1999, ApJ, 510, 874
Papadakis I.E., Nandra K., Kazanas D., 2001, ApJ, 554, L133
Papadakis I.E., Lawrence A., 1995, MNRAS, 272, 161
Peterson B. M., Wanders I., Horne K., Collier S., Alexander T., Kaspi S., Maoz D., 1998, PASP, 110, 660
Pian E. et al., 1998, ApJ, 492, L17
Poutanen J., 2001, Adv. Space Res., 28, 267
Poutanen J., Fabian A.C., 1999, MNRAS, 306, L31
Smith I.A., Liang E.P., 1999, ApJ, 519, 771
Takahashi T. et al., 2000, ApJ, 542, L105
Tanihata C., Urry C.M., Takahashi T., Kataoka J., Wagner S.J., Madejski G.M., Tashiro M., Kouda M., 2001, ApJ, 563, 569
Tavecchio F. et al., 2001, ApJ, 554, 725
Tavecchio F., Maraschi L., Ghisellini G., 1998, ApJ, 509, 608
Timmer J., König M., 1995, A&A, 300, 707
Urry C.M., Padovani P., 1995, PASP, 107, 803
Welsh W.F., 1999, PASP, 111, 1347
White R.J., Peterson B.M., 1994, PASP, 106, 879
Zhang Y.H. et al., 2002, ApJ, 572, 762
Zhang Y.H. et al., 1999, ApJ, 527, 719